

## Ocean Response to Wind Variations, Warm Water Volume, and Simple Models of ENSO in the Low-Frequency Approximation

ALEXEY V. FEDOROV

*Yale University, New Haven, Connecticut*

(Manuscript received 20 January 2009, in final form 22 February 2010)

### ABSTRACT

Physical processes that control ENSO are relatively fast. For instance, it takes only several months for a Kelvin wave to cross the Pacific basin ( $T_k \approx 2$  months), while Rossby waves travel the same distance in about half a year. Compared to such short time scales, the typical periodicity of El Niño is much longer ( $T \approx 2\text{--}7$  yr). Thus, ENSO is fundamentally a low-frequency phenomenon in the context of these faster processes. Here, the author takes advantage of this fact and uses the smallness of the ratio  $\epsilon_k = T_k/T$  to expand solutions of the ocean shallow-water equations into power series (the actual parameter of expansion also includes the oceanic damping rate). Using such an expansion, referred to here as the low-frequency approximation, the author relates thermocline depth anomalies to temperature variations in the eastern equatorial Pacific via an explicit integral operator. This allows a simplified formulation of ENSO dynamics based on an integro-differential equation. Within this formulation, the author shows how the interplay between wind stress curl and oceanic damping rates affects 1) the amplitude and periodicity of El Niño and 2) the phase lag between variations in the equatorial warm water volume and SST in the eastern Pacific. A simple analytical expression is derived for the phase lag. Further, applying the low-frequency approximation to the observed variations in SST, the author computes thermocline depth anomalies in the western and eastern equatorial Pacific to show a good agreement with the observed variations in warm water volume. Ultimately, this approach provides a rigorous framework for deriving other simple models of ENSO (the delayed and recharge oscillators), highlights the limitations of such models, and can be easily used for decadal climate variability in the Pacific.

### 1. Introduction

Interactions between the tropical ocean and the atmosphere produce El Niño–Southern Oscillation (ENSO)—the dominant mode of climate variability in the tropics. This climate phenomenon causes a nearly adiabatic, horizontal redistribution of warm surface water along the equator: during an El Niño, weakened zonal winds permit the warm water to flow eastward so that the ocean thermocline becomes more horizontal, which induces warm SST anomalies in the east. Strong zonal winds during La Niña years pile up the warm water in the west, causing the thermocline slope to increase and exposing cold water to the surface in the east. This zonal adjustment is accompanied by meridional mass redistribution. Numerous studies over the past decades (e.g., Wang et al. 2004;

Clarke 2008; Fedorov et al. 2003) have produced a hierarchy of models describing ENSO, including general circulation models (GCMs) that simulate El Niño with a good degree of fidelity (Guilyardi et al. 2009).

Despite the increasing availability and better performance of ocean–atmosphere GCMs, a large share of our understanding of El Niño still comes from intermediate coupled models based on the shallow-water equations of the ocean (as in Zebiak and Cane 1987). To a large degree, this is because the ocean response to slow (low frequency) wind variations plays a key role in explaining El Niño, and shallow-water models reproduce this response rather accurately.

A class of even simpler models, based on one or several ordinary differential equations that typically describe changes in SSTs in the eastern equatorial Pacific and variations in the depth of the equatorial thermocline, is also critical to our understanding of El Niño. These models include the broadly used delayed (Battisti and Hirst 1989; Suarez and Schopf 1988) and recharge oscillators (Jin 1997a,b; Jin and An 1999; Meinen and

---

*Corresponding author address:* Alexey Fedorov, Dept. of Geology and Geophysics, Yale University, 210 Whitney Ave., New Haven, CT 06511.  
E-mail: alexey.fedorov@yale.edu

McPhaden 2000; Kessler 2003; Clarke et al. 2007; also Philander and Fedorov 2003; Fedorov and Brown 2009). For a summary and brief description of other simple models, see Wang (2001). Some of these models are based on fairly different physical assumptions of the key mechanisms involved; others use different means to represent ocean adjustment.

While conceptual models are extremely valuable for understanding ENSO dynamics, their derivations usually involve either ad hoc assumptions or approximations that cannot be rigorously justified. For example, the delayed oscillator equation is based on a time delay that is not clearly defined. Similarly, the recharge oscillator employs simplifying assumptions for ocean adjustment that are difficult to justify mathematically. Consequently, such models reproduce the full ENSO physics only with limited accuracy as compared to coupled GCMs (Mechoso et al. 2003). The goal of the present study is to circumvent these problems by developing a method of solving the shallow-water equations via a perturbation expansion in terms of a small parameter.

The main idea of this method is to take advantage of the slow, low-frequency essence of the ENSO cycle—slow relative to a number of fast physical processes involved in this phenomenon. In fact, ENSO-related climate variability is characterized by a spectral peak at periods between  $T = 2$  and 7 yr, but the time scales associated with the low-order, dynamically important equatorial waves and other equatorial processes are much shorter. For instance, it takes  $T_k = 2\text{--}3$  months for free baroclinic equatorial Kelvin waves to cross the Pacific basin (and less than 7–8 months for first-mode baroclinic Rossby waves).

Accordingly, we will treat all variables as functions of a small parameters  $\varepsilon$ —a complex number made up by combining  $\varepsilon_k = T_k/T$  and the nondimensional oceanic damping rate  $\varepsilon_m$  (typically, both numbers are small:  $\varepsilon_k, \varepsilon_m \sim 0.05\text{--}0.10$ ). The new parameter will be used for solving the shallow-water equations via an expansion procedure. Since  $\varepsilon_k$  is proportional to the characteristic frequency of ENSO, we will refer to this approach as the low-frequency approximation or limit. This limit will describe the net adjustment of the ocean (rather than propagation of separate waves) and provide an alternative to the method of solving the shallow-water equations by means of parabolic cylinder functions describing Kelvin and Rossby waves of different modes (Battisti 1988; Fedorov and Brown 2009).

This expansion will allow us to derive a new model of ENSO based on a simple integro-differential equation for temperature variations in the eastern equatorial Pacific. This model will offer a quantitatively more rigorous alternative to the conventional simple models of ENSO

(the delayed and recharge oscillators), will provide a mathematical framework for deriving those two models and, at the same time, highlight their limitations.

As part of the low-frequency approximation, we will also obtain explicit expressions for anomalies in the mean thermocline depth, and thermocline anomalies in the eastern and western equatorial Pacific, as functions of temperature in the eastern equatorial Pacific. We will then calculate these anomalies using the observed SST and compare them with the observed variations in the warm water volume (WWV) in the west, east and entire equatorial basin; the results will show a good agreement with the observations.

The volume of water warmer than 20°C, also known as the basinwide equatorial WWV, is an important indicator of the ocean heat recharge and a key element of ENSO dynamics. The WWV typically increases approximately six months to one year in advance of an El Niño event. Our method will allow us to compute the expected phase lag between the ocean recharge (the mean depth of the equatorial thermocline in the model) and SST variations in the eastern equatorial Pacific. We will derive an analytical expression for the phase lag as a function of the oscillation frequency, oceanic damping rates, and the curl of wind stress anomalies. As we will show, the lag can vary in a broad range for these variables. For typical ocean parameters and the oscillation period  $T = 4$  yr, the model predicts the phase lag of about 60°.

Note that the term “low frequency” appears in relation to ENSO in several different contexts. Cane and Moore (1981) used it to distinguish a simplified version of the shallow-water equations with the meridional acceleration neglected, which eliminates short eastward-propagating Rossby waves; this approximation is now commonly called the long-wave or long-wavelength approximation (McCreary 1985). Clarke (1992) studied the low-frequency reflection of Kelvin waves from the eastern boundary and assumed that the wave frequency was small with respect to parameters related to the basin geometry. Jin (2001) used the term “very low frequency” to describe free modes of the system (no wind stress forcing applied) in the absence of explicit damping. In the present study, we use the term low frequency to emphasize that the oscillation frequency is small with respect to time scales associated with Kelvin wave propagation and other fast processes [there are similarities here with the recent study of Clarke (2010)].

The structure of the paper is as follows. In section 2 we formulate the problem. In sections 3 and 4, we describe the expansion procedure for solving the shallow-water equations. The SST equation is discussed in section 5, whereas section 6 combines all relevant equations into a simple ENSO model in the low-frequency limit. In

section 7 we derive the delayed and recharge oscillators from the new model. Section 8 discusses variations in the thermocline depth (and the WWV of the equatorial Pacific). Section 9 concludes the paper.

## 2. Formulation

The ocean dynamics relevant to ENSO can be described by the linear reduced-gravity shallow-water equations on the equatorial  $\beta$  plane in the long-wave approximation (Cane and Sarachik 1981). For simplicity, symmetry with respect to the equator and no annual forcing are assumed:

$$u_t + g'h_x - \beta yv = \tau/\rho D - \varepsilon_m u, \quad (2.1)$$

$$g'h_y + \beta yu = 0, \quad \text{and} \quad (2.2)$$

$$h_t + H(u_x + v_y) = -\varepsilon_m h. \quad (2.3)$$

The notations are conventional, with  $u = u(x, y, t)$  and  $v = v(x, y, t)$  denoting the ocean zonal and meridional currents, respectively;  $H$  is the mean depth of the thermocline,  $h = h(x, y, t)$  are the thermocline depth anomalies;  $\tau = \tau(x, y, t)$  are the zonal components of the wind stress;  $\rho$  is the mean water density;  $\Delta\rho$  is the difference between the density of the upper (warm) layer and the density of the deep lower layer; and  $g' = g\Delta\rho/\rho$  is the reduced gravity. Here  $D$  is the nominal depth, characterizing the effect of surface winds on the ocean thermocline (frequently, it is assumed that  $D = H$ ). The subscripts  $t$ ,  $x$ , and  $y$  indicate the respective derivatives.

The system includes simple Rayleigh friction in the first momentum equation and a linear parameterization of water entrainment at the base of the mixed layer in the continuity equation. The same oceanic damping rate  $\varepsilon_m$  is routinely used in both equations (e.g., Zebiak and Cane 1987; Battisti and Hirst 1989).

We now nondimensionalize these equations using several characteristic scales: the zonal coordinate is scaled by the basin width  $L$ ; the meridional coordinate is scaled by the equatorial Rossby radius of deformation  $L_R = (c/\beta)^{1/2}$ , where  $c = (g'H)^{1/2}$  is the phase velocity of linear baroclinic Kelvin waves; and time is scaled using the basin crossing time for the Kelvin wave,  $T_k = L/c_k$ . Some typical values for the tropical Pacific ocean are  $\Delta\rho/\rho = 0.006$ ;  $L = 150^\circ$ ;  $H = 120$  m;  $D = 75$  m;  $c_k = 2.7$  m s $^{-1}$ ;  $L_R = 340$  km;  $T_k = 2.4$  months; and  $\varepsilon_m = 2.0$  yr $^{-1}$  (Table 1).

The nondimensionalization is completed by substituting the following the equations into the shallow-water Eqs. (2.1)–(2.3):

TABLE 1. Standard parameters used in the shallow-water equations for the tropical Pacific and the SST equation in the equatorial strip.

Parameter	Dimensional	Nondimensional
Basin size $L$	$150^\circ$	1
Kelvin wave speed $c_k$	$2.7$ m s $^{-1}$	1
Basin crossing time $T_k$	2.4 months	1
Basin western boundary $x_w$	$130^\circ\text{E}$	0
Rossby radius of deformation $L_R$	340 km	1
Oceanic damping rate $\varepsilon_m$	$2$ yr $^{-1}$	0.1
Location of the wind maximum $x_c$	$170^\circ\text{W}$	0.4
Wind stress amplitude $\tau_o$	$0.02$ N m $^{-2}$ °C $^{-1}$	$0.62$ (°C) $^{-1}$
$H$	120 m	1
$D$	75 m	0.63
Wind extent parameter $\nu$	$(30^\circ)^{-2}$	25
Wind extent parameter $\alpha$	$(9^\circ)^{-2}$	0.12
Thermal damping rate $\varepsilon_T$	$(125$ days) $^{-1}$	0.57
$d$	50 m	0.42
$\Delta$	$8$ m °C $^{-1}$	$0.067$ °C $^{-1}$
$w_e$	$1$ m day $^{-1}$	0.6
$\gamma_o$	0.5	0.5

$$u \rightarrow u \times c_k \quad v \rightarrow v \times c_k (L_R/L) \quad h \rightarrow h \times H, \quad (2.4)$$

$$x \rightarrow x \times L \quad y \rightarrow y \times L_R \quad t \rightarrow t \times L/c_k, \quad \text{and} \quad (2.5)$$

$$\tau \rightarrow \tau \times \rho c_k^2 (D/L) \quad \varepsilon_m \rightarrow \varepsilon_m \times c_k/L_R. \quad (2.6)$$

Using the same notations for the nondimensional variables, we rewrite the system as

$$u_t + h_x - yv = \tau - \varepsilon_m u, \quad (2.7)$$

$$h_y + yu = 0, \quad \text{and} \quad (2.8)$$

$$h_t + u_x + v_y = -\varepsilon_m h. \quad (2.9)$$

The standard no-flow boundary condition is applied at the eastern ocean boundary ( $x = 1$ ), and the no-net-flow condition at the western boundary ( $x = 0$ ) of the basin (see Cane and Sarachik 1977):

$$\int_{-\infty}^{\infty} u|_{x=0} dy = 0 \quad \text{and} \quad (2.10)$$

$$u|_{x=1} = 0. \quad (2.11)$$

Following Münnich et al. (1991), Jin and Neelin (1993) and other authors, we adopt a simple model for surface winds, in which the wind stress  $\tau = \tau(x, y, t)$  is related to the SST anomaly at the equator  $T = T(x, t)$  through a linear relation,

$$\tau = A(x, y) \cdot T, \quad (2.12)$$

where  $A(x, y)$  is a linear integral operator. Following Jin (1997a,b), we adopt the simplest form of the operator  $A(x, y)$ , taking

$$\tau = \tau_o G(x) e^{-\alpha y^2} T_e, \quad (2.13)$$

where

$$G(x) = e^{-\nu(x-x_c)^2}, \quad (2.14)$$

$T_e = \langle T \rangle$  is the temperature anomaly in the eastern Pacific (e.g., averaged over the Niño-3 region), and  $G(x)$  approximates the shape of the zonal wind stress anomaly along the equator.

We will refer to  $\alpha$  as the wind stress curl parameter, since the curl of wind stress anomalies  $-\partial\tau/\partial y$  is proportional to  $\alpha$ , which makes this parameter critical for assessing meridional water exchange important for ENSO dynamics. We could also refer to  $\alpha$  as the meridional wind extent parameter. The meridional  $e$ -folding decay scale of wind stress anomalies is proportional to  $\alpha^{-1/2}$ , so that for larger  $\alpha$ , wind anomalies are confined closer to the equator.

The typical nondimensional values for the wind stress parameters  $\alpha$ ,  $\nu$ , and  $\tau_o$  (Table 1) correspond to the meridional  $e$ -folding decay scale of roughly  $9^\circ$  of latitude,  $30^\circ$  of longitude for the zonal decay, and the wind stress amplitude of  $0.02 \text{ N m}^{-2} \text{ }^\circ\text{C}^{-1}$ , respectively. These values can be obtained by regressing observed wind stress anomalies onto the Niño-3 SST (Fig. 1; also Wittenberg 2004).

Now, formally applying the Fourier transform to  $h$ ,  $u$ ,  $v$ , and  $\tau$  in Eqs. (2.7)–(2.13), that is, calculating integrals

$$\frac{1}{2\pi} \int_{-\infty}^{\infty} (\dots) e^{-i\omega t} dt \quad (2.15)$$

and using the same notations as those used for the original variables, we obtain

$$\varepsilon u + h_x - yv = \tau, \quad (2.16)$$

$$h_y + yu = 0, \quad \text{and} \quad (2.17)$$

$$\varepsilon h + u_x + v_y = 0, \quad (2.18)$$

where

$$\varepsilon = \varepsilon_m + i\omega. \quad (2.19)$$

Note that a number of studies invoked the fast-wave approximation or limit to describe ENSO. In that limit

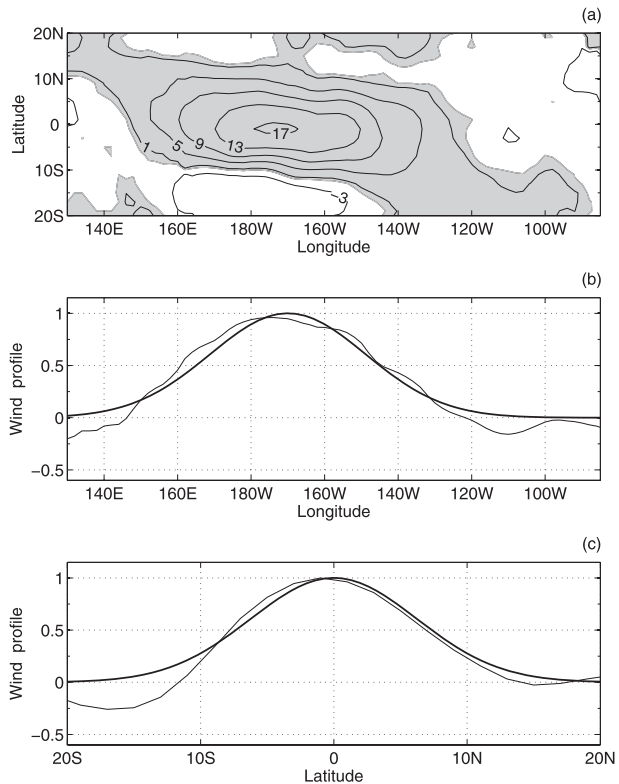


FIG. 1. (a) A regression of the observed wind stress variations onto SST averaged over the eastern equatorial Pacific (defined here as the eastern half of the basin), in units of  $10^{-3} \text{ N m}^{-2} \text{ }^\circ\text{C}^{-1}$  and based on the Florida State University pseudostress (Stricherz et al. 1997; also see Wittenberg 2004). (b) The normalized zonal structure of the observed wind stress anomalies (averaged between  $5^\circ\text{S}$  and  $5^\circ\text{N}$ ) and the model (heavier line). (c) The normalized meridional structure of the observed wind stress anomalies (averaged between  $150^\circ\text{E}$  and  $130^\circ\text{W}$ ) and the model (heavier line). The nondimensional model parameters are  $\nu = 25$ ,  $\alpha = 0.12$ , and  $x_c = 0.4$ .

the speed of Rossby and Kelvin waves is assumed infinite, which implies an instantaneous adjustment of the thermocline to wind stress anomalies (Neelin 1991; Hao et al. 1993; Cane 1992; Galanti and Tziperman 2000). Formally, it would be equivalent to setting  $\omega$  to zero in Eq. (2.19). In this study, we assume that  $\omega$  is nonzero, albeit small. Only when considering the ocean response to steady winds will we set  $\omega = 0$ .

It can be easily shown that Eqs. (2.16)–(2.18) can be rewritten as

$$h_x - \varepsilon y^2 h = \tau - y\tau_y + \varepsilon(yu_y - u), \quad (2.20)$$

$$u = -h_y/y, \quad \text{and} \quad (2.21)$$

$$v = -\tau_y + \varepsilon(yh + u_y). \quad (2.22)$$

The very last equation of this system, Eq. (2.22), is a modified form of the Sverdrup balance that determines

the meridional flow given the wind stress [note that nonlinear terms can become important for this balance in the vicinity of the equator; see Brown and Fedorov (2010a)]. An additional equation for SSTs will be needed to close the system (as described in section 5).

### 3. Singular perturbation expansion for the shallow-water equations

Now we will solve Eqs. (2.20) and (2.21) using a perturbation method that assumes, for the time of derivation, that  $\varepsilon$  is a constant. This approach is frequently used in theoretical physics, when deriving the nonlinear Schrödinger equation or other evolutionary equations for ocean surface waves, for example (e.g., Zakharov 1968). It can be applied as long as the spectrum of the process under consideration has a relatively narrow peak; in other words, only when a limited range of  $\varepsilon$  close to the maximum of the spectrum is relevant for the problem.

We will assume that the wind stress and thermocline depth anomalies vary on time scales much longer than the time needed for a free Kelvin wave to cross the Pacific and that oceanic damping is relatively weak, which implies that  $|\varepsilon| \ll 1$ .

We rewrite the system of governing equations as

$$h_x - \varepsilon y^2 h = (1 - y\partial_y)\tau - \varepsilon(1 - y\partial_y)u \quad \text{and} \quad (3.1)$$

$$u = -h_y/y. \quad (3.2)$$

It is crucially important for our approach that the second term on the left-hand-side of Eq. (3.1) be formally considered of the same order as the first term; this is because  $\varepsilon y^2 h$  can become sufficiently large for large  $|y|$ . In fact, it is exactly the part of the equation that accounts for the delayed ocean adjustment to wind variations (ocean memory, e.g.; Neelin et al. 1998; Fedorov and Brown 2009). In other words, these equations represent a singular perturbation problem.

Also, technically we should consider solutions in the ocean basin bounded by the condition  $|y| < Y$ , where  $Y \sim \varepsilon^{-1/2}$ , which would keep the second term on the left-hand-side of Eq. (3.1) bounded and not larger than  $O(1)$ . However, it turns out that the solutions for  $h$  decay exponentially for large  $|y|$ , as long as  $x \neq 1$ , so that this requirement is not critical.

Now we can formally expand  $h$  and  $u$  in powers of  $\varepsilon$ , assuming that  $|\varepsilon|$  is a small parameter:

$$h = h^{(0)} + h^{(2)} + \dots \quad \text{and} \quad (3.3)$$

$$u = u^{(1)} + u^{(3)} + \dots, \quad (3.4)$$

where the terms in Eqs. (3.3) and (3.4) are proportional to powers of  $\varepsilon$ , as indicated by the superscripts. As shown in appendix A, the terms in Eq. (3.3) proportional to odd powers of  $\varepsilon$  and the terms in Eq. (3.4) proportional to even powers of  $\varepsilon$  are identically zero.

Accordingly, the zeroth-order solution for  $h$  (and the first order for  $u$ ) will satisfy two simple equations:

$$h_x^{(0)} - \varepsilon y^2 h^{(0)} = (1 - y\partial_y)\tau \quad \text{and} \quad (3.5)$$

$$u^{(1)} = -h_y^{(0)}/y. \quad (3.6)$$

Integrating Eqs. (3.5) and (3.6) gives

$$h^{(0)} = e^{\varepsilon y^2(x-1)} h_o - \int_x^1 e^{\varepsilon y^2(x-s)} (1 - y\partial_y)\tau(s, y) ds \quad \text{and} \quad (3.7)$$

$$u^{(1)} = 2\varepsilon(1-x)e^{\varepsilon y^2(x-1)} h_o - \int_x^1 e^{\varepsilon y^2(x-s)} [\partial_{yy} + 2\varepsilon(s-x)(1-y\partial_y)]\tau(s, y) ds, \quad (3.8)$$

where  $h_o$  is the thermocline depth anomaly at the eastern boundary ( $x = 1$ ) and the no-flow condition has been already applied (for the higher-order terms of the expansion, see appendix A).

Using the no-net-flow condition at the western boundary ( $x = 0$ ) and integration by parts give

$$h_o = \int_0^1 \int_{-\infty}^{\infty} \tau e^{-\varepsilon y^2 x} x dx dy / \int_{-\infty}^{\infty} e^{-\varepsilon y^2} dy = \pi^{-1/2} \varepsilon^{1/2} \int_0^1 \int_{-\infty}^{\infty} \tau(x, y) e^{-\varepsilon y^2 x} x dx dy. \quad (3.9)$$

Since the prescribed meridional shape of wind stress anomalies is such that

$$\tau(x, y) = \tau(x) e^{-\alpha y^2}, \quad (3.10)$$

we can integrate Eq. (3.9) once to obtain

$$h_o = \int_0^1 \tau(x) x \sqrt{\frac{\varepsilon}{\varepsilon x + \alpha}} dx, \quad (3.11)$$

where

$$\tau(x) = \tau(x, y)|_{y=0}. \quad (3.12)$$

Formally, Eq. (3.11) is similar to the expression for the thermocline depth at the eastern boundary in the “fast-wave limit” (as discussed in Hao et al. 1993; also Cane

and Sarachik 1981; Cane et al. 1990), but here  $\varepsilon$  incorporates the frequency  $\omega$ , not just oceanic damping. In general, one would need to specify the branch of the square root in Eq. (3.11), but this will not alter the end results.

In principle, one could further expand the expression for  $h_o$  in Eq. (3.11), assuming that  $|\varepsilon|$  is small; however, in practice  $|\varepsilon|$  and  $\alpha$  can be of the same order, making it necessary to find a different approach to simplify Eq. (3.11). Since wind stress anomalies are confined to the western and central equatorial Pacific and  $\tau(x)$  is localized in the vicinity of  $x_c$  (the location of the maximum of wind stress anomalies), with a good accuracy we can replace Eq. (3.11) with

$$h_o = \sqrt{\frac{\varepsilon}{\varepsilon x_c + \alpha}} \int_0^1 \tau(x) x \, dx. \quad (3.13)$$

This expression will be used in a simple model of ENSO discussed shortly.

Next, using Eq. (3.10) we arrive at the following equations for  $h$  and  $u$ :

$$h = e^{\varepsilon y^2(x-1)} h_o - \int_x^1 \tau(s)(1 + 2\alpha y^2) e^{\varepsilon y^2(x-s)-\alpha y^2} \, ds \quad \text{and} \quad (3.14)$$

$$u = 2\varepsilon(1-x)e^{\varepsilon y^2(x-1)} h_o - \int_x^1 \tau(s)[-2\alpha + 4\alpha^2 y^2 + 2\varepsilon(s-x)(1+2\alpha y^2)] e^{\varepsilon y^2(x-s)-\alpha y^2} \, ds. \quad (3.15)$$

To understand the properties of the solutions described by Eqs. (3.14) and (3.15), let us assume that the wind stress forcing is proportional to  $\text{Re}(e^{i\omega t})$  and that the oscillation frequency  $\omega$  is fixed. Then the spatial structure of the thermocline at two instances separated by a quarter period of the oscillation is given by  $\text{Re}(h)$  and  $\text{Im}(h)$ , where  $h$  can be calculated from Eq. (3.14). In an example shown in Fig. 2, thermocline depth anomalies are forced by wind variations with  $T = 4$  yr. The ocean damping time scale was set to 2 yr (nondimensional  $\varepsilon_m = 0.1$ ), consistent with estimates by Fedorov (2007) and Brown and Fedorov (2010b).

The spatial patterns of the thermocline depth anomalies are easy to recognize. In fact, Figs. 2a and 2b show typical thermocline anomalies during and preceding an El Niño event, respectively. The agreement between these solutions and those obtained from the full shallow-water equations (not shown) is nearly perfect. Figure 2b also clearly demonstrates the ocean warm water recharge, that is, the deepening of the equatorial thermocline preceding El Niño.

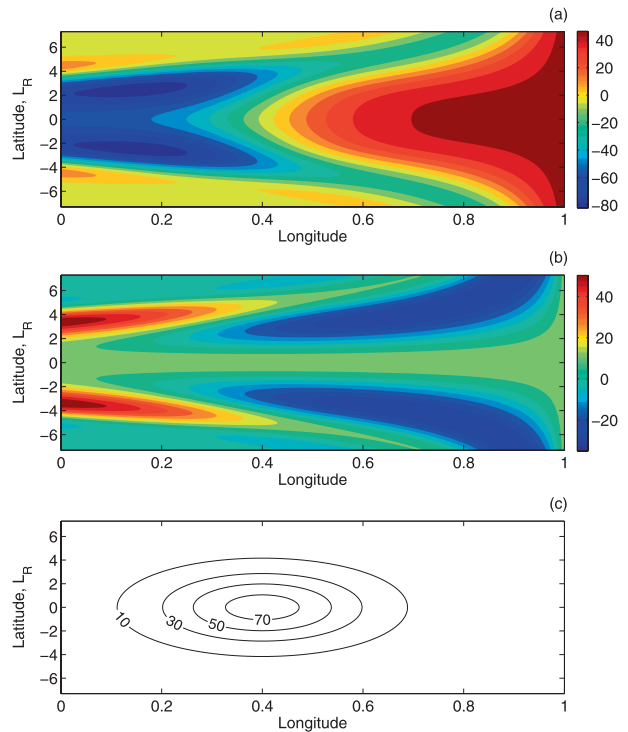


FIG. 2. The leading-order response of the ocean thermocline to wind stress variations for  $T = 4$  yr: (a)  $\text{Re}(h)$ , (b)  $\text{Im}(h)$ , (c) wind stress anomaly  $\tau$  at its peak. The complex expression for  $h$  is given by Eqs. (3.11) and (3.14); the wind stress is given by Eqs. (2.13) and (2.14). Thermocline depth is in meters, wind stress in units of  $10^{-3}$  N m $^{-2}$ . The amplitude of the temperature anomaly  $T_e$  is set to 4°C, corresponding to a strong El Niño. Plots (a) and (b) can be interpreted as thermocline displacements at two different instances: one corresponding to an El Niño state with a reduced thermocline slope along the equator and the other describing a recharged state with the mean equatorial thermocline deeper than normal by approximately 10 m, respectively. The ocean state in (a) lags that in (b) by a quarter period. Longitude and latitude are nondimensionalized using the basin length and the Rossby radius of deformation, respectively. Note the typical forced quasistationary Rossby and Kelvin wave patterns. The nondimensional parameters are  $\varepsilon_m = 0.1$ ,  $\tau_o = 0.6$ ,  $\alpha = 0.12$ ,  $x_c = 0.4$ , and  $\nu = 25$ .

#### 4. Thermocline depth variations along the equator

Next, we will focus on thermocline variations along the equator. Accordingly, to the leading order at the equator ( $y = 0$ ),

$$\begin{aligned} h &= h(x) = h_o - \int_x^1 \tau(s) \, ds \\ &= \sqrt{\frac{\varepsilon}{\varepsilon x_c + \alpha}} \int_0^1 \tau(s) s \, ds - \int_x^1 \tau(s) \, ds. \end{aligned} \quad (4.1)$$

Since wind stress anomalies along the equator are proportional to  $\tau_o G(x) T_e$ , we can rewrite Eq. (4.1) as

$$h = \tau_o \left( q \sqrt{\frac{\varepsilon}{\varepsilon x_c + \alpha}} + R \right) T_e \quad \text{with} \quad (4.2) \quad h_e = \tau_o r T_e + \frac{\tau_o q}{\sqrt{x_c}} \left[ T_e + \frac{1}{\pi} \int_0^\infty e^{-\varepsilon_m t'} I(\hat{\alpha}, t') T_e(t - t') dt' \right], \quad (4.12)$$

$$R = R(x) = - \int_x^1 G(s) ds \quad \text{and} \quad (4.3) \quad \text{where}$$

$$q = \int_0^1 G(s) s ds. \quad (4.4) \quad I(\hat{\alpha}, t) = \frac{d}{dt} I_1(\hat{\alpha}t) = -\hat{\alpha} \int_0^1 e^{-\hat{\alpha}ts} \sqrt{\frac{s}{1-s}} ds. \quad (4.13)$$

Averaging Eq. (4.2) over the eastern equatorial Pacific (e.g., over the Niño-3 region) gives

$$h_e = \tau_o \left( r + q \sqrt{\frac{\varepsilon}{\varepsilon x_c + \alpha}} \right) T_e, \quad (4.5)$$

where

$$h_e = \langle h \rangle = \frac{1}{l_e} \int_{1-l_e}^1 h dx \quad \text{and} \quad (4.6)$$

$$r = \langle R \rangle = \frac{1}{l_e} \int_{1-l_e}^1 R dx \quad (4.7)$$

and  $[1 - l_e, 1]$  is the averaging interval. Equation (4.5) will be used for deriving a simple model of ENSO in the next sections. The values of  $q$  and  $r$  depend only weakly on relevant parameters ( $\nu$  and  $x_c$ ). For the standard choice of parameters given in Table 1 and  $l_e = 1/2$ , we compute  $q = 0.142$  and  $r = -0.014$ .

To go back to the time-dependent variables, we will now use the inverse Fourier transform, the convolution theorem, and the integral

$$\begin{aligned} \int_{-\infty}^{\infty} \frac{e^{i\omega t}}{\sqrt{\varepsilon(\varepsilon + \hat{\alpha})}} d\omega &= - \int_{-\infty}^{\infty} \frac{i e^{i\omega t} d\omega}{\sqrt{(\omega - i\varepsilon_m)(\omega - i\varepsilon_m - i\hat{\alpha})}} \\ &= 2\theta(t) e^{-\varepsilon_m t} I_1(\hat{\alpha}t), \end{aligned} \quad (4.8)$$

where

$$I_1(\hat{\alpha}t) = \int_0^1 \frac{e^{-\hat{\alpha}ts}}{\sqrt{s(1-s)}} ds \quad \text{and} \quad (4.9)$$

$$\hat{\alpha} = \alpha/x_c, \quad (4.10)$$

and  $\theta(t)$  is the step function. Using the same notations for the corresponding variables, we convert (4.5) into

$$h_e = \tau_o r T_e + \frac{\tau_o q}{\pi \sqrt{x_c}} (\partial_t + \varepsilon_m) \int_0^\infty e^{-\varepsilon_m t'} I_1(\hat{\alpha}t') T_e(t - t') dt'. \quad (4.11)$$

Further simplifications and applying the identity  $I_1(0) = \pi$  give

As shown in appendix B, the integral  $I(\hat{\alpha}, t)$  behaves asymptotically for large  $t$  as

$$I(\hat{\alpha}, t) \sim -\frac{1}{2} \left( \frac{\pi x_c}{\alpha} \right)^{1/2} t^{-3/2}. \quad (4.14)$$

The parameter  $\alpha$  being in the denominator of Eq. (4.14) emphasizes that this result is critically dependent on the nonzero wind stress curl.

We can rewrite Eq. (4.12) as

$$\begin{aligned} h_e &= \tau_o q \left[ \left( \frac{r}{q} + \frac{1}{\sqrt{x_c}} \right) T_e \right. \\ &\quad \left. + \frac{1}{\pi \sqrt{x_c}} \int_0^\infty e^{-\varepsilon_m t'} I(\hat{\alpha}, t') T_e(t - t') dt' \right]. \end{aligned} \quad (4.15)$$

This is the central result of this section. The first term on the right-hand side of Eq. (4.15) gives rise to the Bjerknes feedback, that is, weaker zonal winds lead to a deeper thermocline in the eastern equatorial Pacific, warmer SSTs there, and even weaker winds (e.g., Fedorov 2002). The second term describes the slow ocean adjustment. By virtue of this expression, the thermocline depth in the eastern equatorial Pacific depends at time  $t$  both on the instantaneous temperature  $T_e(t)$  and on temperatures integrated over a time interval preceding this instance. The duration of this interval is determined by the rate with which the kernel in Eq. (4.15) decays for large  $t$  and is controlled by the oceanic damping rate  $\varepsilon_m$  and the parameter  $\alpha/x_c$ .

## 5. The SST equation

To derive a simple model of ENSO, one would need an additional equation describing changes in sea surface temperatures. Following Jin and Neelin (1993), we approximate the dynamics of SST anomalies along the equatorial strip with a linearized equation in which the rate of temperature change is balanced by the mean upwelling and thermodynamic damping:

$$T_t + \bar{w} T_z = -\varepsilon_T T. \quad (5.1)$$

Here,  $\bar{w}$  is the time-mean vertical velocity in the equatorial strip and  $\varepsilon_T$  is thermal damping. We have neglected the effects of anomalous upwelling and zonal and meridional advection. These additional terms can be easily added to the model. Variables in this equation (except for temperature  $T$ ) are nondimensionalized using time  $T_k$  as the temporal scale,  $H$  as the scale for the vertical coordinate, and  $c_k H/L$  as the scale for the vertical velocity.

The effect of upwelling on the surface temperature is then estimated using a finite difference:

$$T_t + \gamma_o \frac{\bar{w}}{d} (T - T_{\text{ent}}) = -\varepsilon_T T, \quad (5.2)$$

where  $T_{\text{ent}} = T_{\text{ent}}(h)$  is a temperature anomaly entrained at the base of the mixed layer of thickness  $d$ , and  $\gamma_o$  is the efficiency of upwelling. Following Fedorov and Philander (2001), we choose  $d = 50$  m and  $\gamma_o = 0.5$ . Note that Galanti and Tziperman (2000), for instance, chose  $d = 75$  m and  $\gamma_o = 0.75$ , yielding the same ratio  $\gamma_o/d$ .

In the linear approximation, the temperature  $T_{\text{ent}}$  is related to the thermocline depth anomaly  $h$  as

$$T_{\text{ent}} = h \frac{\partial T}{\partial z} \Big|^{z=-d} = \frac{h}{\Delta}, \quad (5.3)$$

where

$$\Delta = \frac{1}{\partial T / \partial z} \Big|^{z=-d}. \quad (5.4)$$

The parameter  $\Delta$  describes the thickness of the tropical thermocline, or more exactly the nondimensional vertical length scale over which the subsurface temperature changes by 1°C. The dimensional value of the mean temperature gradient across the thermocline is set here to  $0.13^\circ\text{C m}^{-1}$ .

Using Eq. (5.3) we can rewrite Eq. (5.2) as

$$T_t + \gamma_o \frac{\bar{w}}{d} \left( T - \frac{h}{\Delta} \right) = -\varepsilon_T T \quad \text{or} \quad (5.5)$$

$$T_t + \left( \gamma_o \frac{\bar{w}}{d} + \varepsilon_T \right) T = \gamma_o \frac{\bar{w} h}{d \Delta}. \quad (5.6)$$

Averaging Eq. (5.6) over the eastern Pacific, neglecting nonlinear terms, and introducing

$$T_e = \langle T \rangle, \quad h_e = \langle h \rangle, \quad w_e = \langle \bar{w} \rangle \quad \text{and} \quad (5.7)$$

$$\varepsilon_w = \gamma_o \frac{w_e}{d}, \quad (5.8)$$

we arrive at the temperature equation

$$\frac{d}{dt} T_e + (\varepsilon_w + \varepsilon_T) T_e = \varepsilon_w \frac{h_e}{\Delta}, \quad (5.9)$$

which describes the dominant temperature tendency in the eastern equatorial Pacific. Other terms, such as zonal advection of temperature or anomalous vertical upwelling, can be easily included in the equation. For future use we also introduce  $\varepsilon_h$  as

$$\varepsilon_h = \tau_o \frac{\varepsilon_w}{\Delta} = \gamma_o \frac{w_e \tau_o}{d} \frac{h_e}{\Delta}. \quad (5.10)$$

The parameter  $\varepsilon_h$  reflects the coupling between thermocline and SST anomalies.

Choosing the appropriate value for the upwelling velocity  $w_e$  in Eqs. (5.7)–(5.10) is not straightforward. Available observational estimates are indirect and typically based on calculating the divergence of horizontal currents. Meinen et al. (2001) evaluated the annual mean vertical velocity at 50-m depth at  $0.3 \pm 0.03 \text{ m day}^{-1}$  when averaged over the region  $5^\circ\text{S}$ – $5^\circ\text{N}$ ,  $155^\circ$ – $95^\circ\text{W}$ . Johnson et al. (2001) estimated, however, that the mean vertical upwelling at 50 m was roughly  $0.7 \pm 0.2 \text{ m day}^{-1}$  when the averaging region is bounded by  $3.6^\circ\text{S}$ – $5.2^\circ\text{N}$ ,  $170^\circ$ – $95^\circ\text{W}$ . Johnson et al. also concluded that the vertical velocity in the vicinity of the equator at 50 m peaked at  $1.6 \pm 0.8 \text{ m day}^{-1}$ . Different ocean analyses give maximum values of upwelling averaged between  $2^\circ\text{S}$  and  $2^\circ\text{N}$  in the range  $1$ – $2 \text{ m day}^{-1}$ , more or less within the error bars of the observations (Behringer et al. 1998, Capotondi et al. 2006).

The averaging in this study will use the area bounded along the equator by  $155^\circ$ – $80^\circ\text{W}$ , which covers the eastern half of the basin, is only slightly different from the Niño-3 region, and is shifted eastward by  $15^\circ$  with respect to the region used by Johnson et al. Averaging within the band  $2^\circ\text{S}$ – $2^\circ\text{N}$  (where most of the upwelling takes place; Brown and Fedorov 2008) appears to be appropriate. Given the uncertainty in the available data, we choose our standard value for the vertical velocity  $w_e = 1 \text{ m day}^{-1}$ , which is lower than used by Galanti and Tziperman (2000) but slightly higher than Johnson et al.'s average value. Choosing a different upwelling rate is partially equivalent to modifying  $\tau_o$  in Eq. (5.10).

## 6. A simple ENSO model in the low-frequency limit

Now we can combine the results of the earlier sections with the SST equation

$$\frac{d}{dt} T_e + (\varepsilon_w + \varepsilon_T) T_e = \varepsilon_w \frac{h_e}{\Delta} \quad (6.1)$$

and obtain a single equation for temperature  $T_e$ :

$$\begin{aligned} \frac{d}{dt} T_e + \left[ \varepsilon_w + \varepsilon_T - \left( r + \frac{q}{\sqrt{x_c}} \right) \varepsilon_h \right] T_e \\ = \frac{q \varepsilon_h}{\pi \sqrt{x_c}} \int_0^\infty e^{-\varepsilon_m t'} I(\hat{\alpha}, t') T_e(t-t') dt'. \end{aligned} \quad (6.2)$$

We rewrite Eq. (6.2) as

$$\frac{d}{dt} T_e + a T_e = b \int_0^\infty e^{-\varepsilon_m t'} I(\hat{\alpha}, t') T_e(t-t') dt', \quad (6.3)$$

$$a = \varepsilon_w + \varepsilon_T - \left( r + \frac{q}{\sqrt{x_c}} \right) \varepsilon_h \quad \text{and} \quad b = \frac{q \varepsilon_h}{\pi \sqrt{x_c}}. \quad (6.4)$$

One can also rewrite Eq. (6.3) as

$$\frac{d}{dt} T_e + a T_e = b K \cdot T_e, \quad (6.5)$$

where  $K$  stands for the integral operator in Eq. (6.3). This is a simple ENSO model that describes variations in the temperature  $T_e$  of the eastern equatorial Pacific with an integro-differential equation. Wind stress curl is essential for this model because of the role of  $\alpha$  in the integral operator.

The right-hand side of Eq. (6.5) gives a rigorous representation of the effect of the delayed response of the thermocline to changes in temperature  $T_e$  over a preceding time interval and hence to past wind variations. There is no explicit representation of Rossby or Kelvin waves in the model, but rather the net oceanic adjustment. The time delay originates from this adjustment and is described by the cumulative effect of past temperature variations on current temperature  $T_e$ .

To calculate the complex frequency  $\sigma = \omega - i\gamma$  of the oscillations that can occur in this system (a positive  $\gamma$  corresponds to unstable oscillations), we substitute  $T_e \sim e^{i\sigma t}$  into Eq. (6.3) and obtain

$$i\sigma + (\varepsilon_w + \varepsilon_T - r\varepsilon_h) = \varepsilon_h q \sqrt{\frac{\varepsilon_m + i\sigma}{(\varepsilon_m + i\sigma)x_c + \alpha}} \quad \text{or} \quad (6.6)$$

$$(i\sigma + \varepsilon_w + \varepsilon_T - r\varepsilon_h)^2 [(\varepsilon_m + i\sigma)x_c + \alpha] = \varepsilon_h^2 q^2 (\varepsilon_m + i\sigma). \quad (6.7)$$

This is a third-order algebraic equation that can be easily solved. Next, we will explore how the solutions of this equation depend on  $\mu$  (the effective coupling strength between the ocean and the atmosphere), on  $\alpha$  (the parameter that controls the meridional structure of the

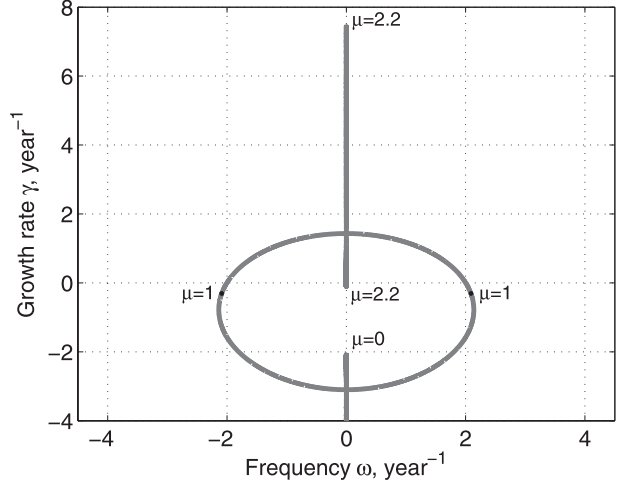


FIG. 3. A bifurcation diagram showing the frequency  $\omega = \text{Re}(\sigma)$  and the growth rate  $\gamma = -\text{Im}(\sigma)$  of the oscillation given by Eq. (6.7) for different values of  $\mu = \tau_o/\tau_{o,\text{standard}}$ , as produced by our simple model in the low-frequency limit. Negative  $\gamma$  indicate damped oscillations. Oscillatory solutions emerge as a consequence of a Hopf bifurcation when  $\mu$  decreases from larger values to roughly  $\mu = 1.6$ . The nondimensional parameters are  $\varepsilon_m = 0.1$ ,  $\alpha = 0.12$ ,  $x_c = 0.4$ , and  $\nu = 25$ . The reference wind stress amplitude  $\tau_{o,\text{standard}} = 0.02 \text{ N m}^{-2} \text{ }^{\circ}\text{C}^{-1}$ . The third family of solutions (not shown) is not physical.

wind stress anomalies and wind stress curl), and on  $\varepsilon_m$  (oceanic damping).

First, we introduce the normalized wind stress amplitude  $\mu = \tau_o/\tau_{o,\text{standard}}$ , which can be interpreted as the effective coupling strength between the ocean and the atmosphere. Figure 3 shows the bifurcation diagram on the  $(\omega, \gamma)$  plane for the physically sound solutions of Eq. (6.7). Oscillatory solutions emerge as a result of a Hopf bifurcation when  $\mu$  is reduced to a proper value. The ellipse corresponding to oscillatory solutions occupies both the upper and lower half-planes, indicating that both growing and decaying oscillations are possible. The range of the coupling strength allowing oscillatory solutions is rather broad:  $\mu \approx 0.3\text{--}1.6$  (Fig. 4).

For  $\mu = 1$ , the model produces a weakly damped oscillation with the period  $T \approx 3 \text{ yr}$  and the damping time scale  $|\gamma| \approx 2 \text{ yr}$  (Fig. 4). Decreasing  $\mu$  leads to stronger damping of the oscillations. Increasing  $\mu$  makes the oscillation unstable and increases its period. At the critical value of  $\mu \approx 1.6$ , the period of the oscillation becomes infinite ( $T \rightarrow \infty$  or  $\omega \rightarrow 0$ ).

As the next step, we fix the coupling strength  $\mu = 1$  and consider the properties of the solutions as a function of the wind stress curl  $\alpha$  and the oceanic damping rate  $\varepsilon_m$ —both are clearly important for the oscillations. Increasing  $\varepsilon_m$  leads to stronger decay rates and longer oscillation periods (Fig. 5). On the other hand, increasing

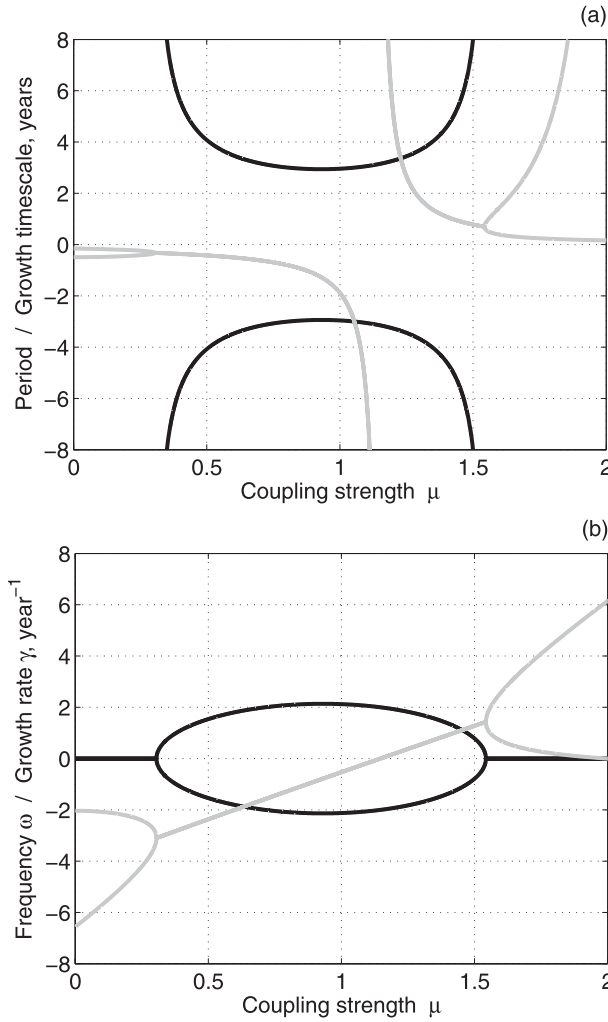


FIG. 4. (a) The period and the growth time scale of the oscillation (heavy and light lines, respectively) as a function of the effective coupling strength  $\mu = \tau_o/\tau_{o,\text{standard}}$ . Negative and positive frequencies produce identical solutions. Negative growth rates (time scales) indicate damped oscillations. (b) The same for  $\omega = \text{Re}(\sigma)$  and  $\gamma = -\text{Im}(\sigma)$  of the oscillations. Relevant parameters are as in Fig. 3. For  $\mu = 1$  the model produces a weakly damped oscillation with  $T \approx 3$  yr and  $\gamma^{-1} \approx -2$  yr. For large values of  $\mu$ , there are no oscillatory solutions.

$\alpha$  (and hence strengthening the wind stress curl) reduces the oscillation period (Figs. 5 and 6). In fact, for larger values of  $\alpha$ —that is, for wind anomalies too narrowly confined about the equator—ENSO becomes nearly biennial. This is consistent with the behavior of coupled GCMs such as Community Climate System Model, version 3 (CCSM3; Deser et al. 2006; Capotondi et al. 2006).

For a broad range of  $\alpha$  and  $\varepsilon_m$ , oscillations remain damped. Only for small values of  $\alpha$  and  $\varepsilon_m$ , one finds growing oscillatory solutions (the lower left corner of Fig. 5b). The boundary between oscillatory and purely

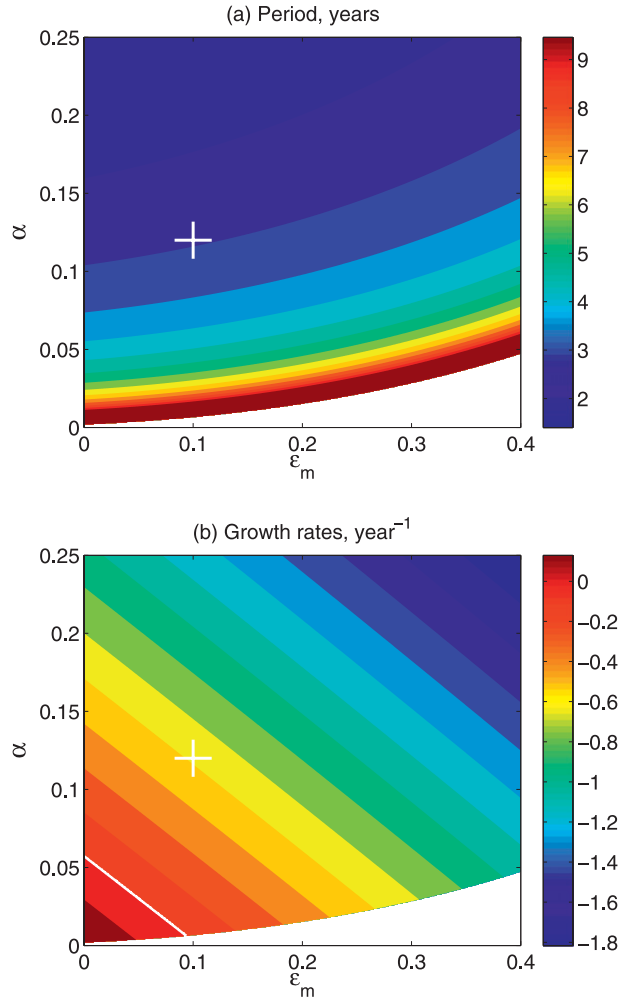


FIG. 5. (a) The period and (b) the growth rates of the ENSO-like solutions as functions of  $\varepsilon_m$  and  $\alpha$ . There are no oscillatory solutions in the white area ( $\omega = 0$ ). The dark red area in (a) indicates periods 10 yr and longer. At the boundary between the dark red and white areas,  $\omega = 0$  ( $T \rightarrow \infty$ ). The white inclined line in (b) corresponds to neutral stability ( $\gamma = 0$ ). The white cross indicates the standard tropical mean state with  $\varepsilon_m = 0.1$  and  $\alpha = 0.12$ , producing a weakly damped oscillation with  $T \approx 3$  yr and  $\gamma^{-1} \approx -2$  yr. The maximum values of  $\varepsilon_m$  and  $\alpha$  in the plot correspond to the oceanic damping time scales of six months and the meridional extent of the wind anomalies of 6°, respectively. For  $x_c = 0.4$  and  $\nu = 25$ . The dimensional wind stress amplitude  $\tau_o = 0.02 \text{ N m}^{-2} \text{ C}^{-1}$  ( $\mu = 1$ ).

growing/decaying solutions in Fig. 5 (colored and white areas, respectively) is given by the condition  $\omega \rightarrow 0$  ( $T \rightarrow \infty$ ).

Increasing the coupling strength  $\mu$ , say, by 25% does not change the character of solutions qualitatively. For the standard combination of  $\alpha$  and  $\varepsilon_m$ , the period  $T$  increases roughly to 3.5 yr and the oscillation becomes weakly unstable with the *e*-folding growth time scale  $\gamma^{-1} \approx 3$  yr (Fig. 4a). The range of  $\alpha$  and  $\varepsilon_m$  with oscillatory

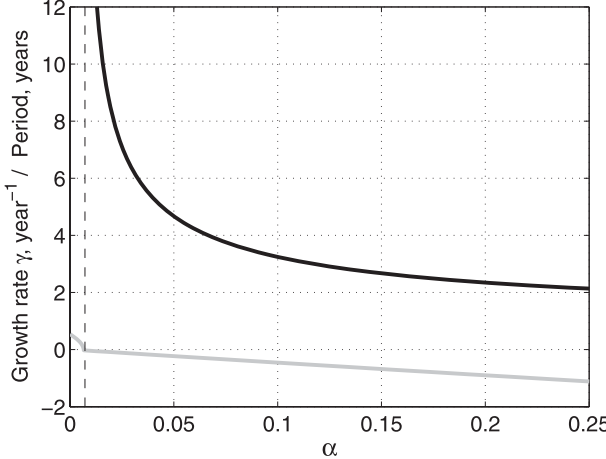


FIG. 6. (a) The period and the growth rate of the oscillation (heavy and light lines, respectively) as functions of  $\alpha$ . Negative  $\gamma$  indicates damped oscillations. There are no oscillatory solutions to the left of the dashed line. The nondimensional parameters are  $\varepsilon_m = 0.1$ ,  $x_c = 0.4$ , and  $\nu = 25$ . The wind stress amplitude  $\tau_o = 0.02 \text{ N m}^{-2} \text{ }^{\circ}\text{C}^{-1}$ .

solutions shrinks; eventually, with further increase in  $\mu$ , oscillatory solutions can no longer exist.

## 7. Relation to the delayed and recharge oscillator models

The main equation of the simple ENSO model derived in the previous sections using the low-frequency approximation is

$$\frac{d}{dt} T_e + aT_e = b \int_0^\infty e^{-\varepsilon_m t'} I(\hat{\alpha}, t') T_e(t-t') dt', \quad (7.1)$$

where  $a$  and  $b$  are constants related to other parameters of the system [see Eq. (6.4)]. This equation has similarities with the delayed oscillator model (Schopf and Suarez 1988; Battisti and Hirst 1989; also Fedorov and Philander 2001); however, it is rigorously derived. The Bjerknes feedback, modified by damping terms, is described by the term proportional to  $a$ . The delayed ocean adjustment is represented by the integral in the right-hand-side of the equation; the wind stress curl and oceanic damping are explicitly included in this latter term.

To obtain the delayed oscillator equation from this model, one can evaluate the integral in Eq. (7.1):

$$\int_0^\infty e^{-\varepsilon_m t'} I(\hat{\alpha}, t') T_e(t-t') dt' \approx B e^{-\varepsilon_m t_o} I(\hat{\alpha}, t_o) T_e(t-t_o), \quad (7.2)$$

where  $t_o$  are  $B$  are constants chosen to give the best fit for this integral. Then Eq. (7.1) can be rewritten as

$$\frac{d}{dt} T_e + aT_e = \tilde{b} T_e(t-t_o), \quad (7.3)$$

where  $\tilde{b}$  is a new constant that has replaced  $b$ . This is the classical linear delayed oscillator, in which  $t_o$  plays the role of the time delay. The problem with such an approach, however, is that the time delay is not clearly defined. It results from an ad hoc approximation for several different processes and actually leads to a degeneracy of this equation. The simple model of Eq. (7.1) avoids this problem by introducing the time delay through an integral operator applied to  $T_e$ .

One can also obtain an equivalent of the recharge oscillator model of ENSO. First, we denote the integral on the right-hand side of Eq. (7.1) as  $W = W(t)$ . This term is related to the warm water volume anomaly or ocean heat recharge in the western Pacific. However, it excludes the portion of the WWV anomaly proportional to  $T_e$  (see section 8). Calculating the time derivative of  $W$  transforms Eq. (7.1) into two equations

$$\frac{d}{dt} T_e + aT_e = bW \quad \text{and} \quad (7.4)$$

$$\frac{d}{dt} W = - \int_0^\infty e^{-\varepsilon_m t'} I(\hat{\alpha}, t') \frac{d}{dt'} T_e(t-t') dt'. \quad (7.5)$$

After integrating by parts, we can approximate the integral in Eq. (7.5) as

$$\begin{aligned} \int_0^\infty e^{-\varepsilon_m t'} I(\hat{\alpha}, t') \frac{d}{dt'} T_e(t-t') dt' &= -I(\hat{\alpha}, 0) T_e(t) \\ &- \int_0^\infty T_e(t-t') \frac{d}{dt'} [e^{-\varepsilon_m t'} I(\hat{\alpha}, t')] dt' \approx -I(\hat{\alpha}, 0) T_e(t). \end{aligned} \quad (7.6)$$

Here, we have neglected the second integral in Eq. (7.6), which is relatively small, but contains all effects of  $\varepsilon_m$ . In appendix B we obtain

$$I(\hat{\alpha}, 0) = -\frac{\pi}{2} \hat{\alpha} = -\frac{\pi \alpha}{2x_c}. \quad (7.7)$$

Now we can reduce the system of Eqs. (7.4) and (7.5) to

$$\frac{d}{dt} T_e + aT_e = bW \quad \text{and} \quad (7.8)$$

$$\frac{d}{dt} W = -cT_e \quad \text{with} \quad (7.9)$$

$$a = \varepsilon_w + \varepsilon_T - \left( r + \frac{q}{\sqrt{x_c}} \right) \varepsilon_h; \quad b = \frac{q \varepsilon_h}{\pi \sqrt{x_c}}; \quad c = \frac{\pi \alpha}{2x_c}. \quad (7.10)$$

These equations are formally similar to the recharge–discharge oscillator model by Jin (1997a,b); however, in a clear improvement, they include a quantitatively rigorous representation of the effect of wind stress curl on the ocean heat recharge [here, there is a direct link with the empirical model for the ocean heat recharge used by Clarke et al. (2007)]. The simplified equations agree well with the full model of Eq. (7.1) in the limit of very small  $\alpha$  and  $\varepsilon_m$  (i.e., in the lower-left corner of the panels in Fig. 5).

Both derivations (of the delayed and recharge oscillators) using our model as a starting point emphasize that these two frequently used conceptual models of ENSO, while reasonable, are based on relatively crude approximations. Therefore, obtaining good quantitative agreement with data from coupled GCMs or observations is often more reliant on the method used to fit the model to the data (e.g., Mechoso et al. 2003).

## 8. Mean thermocline depth and WWV variations

The low-frequency approximation is ideally suited to study variations in the WWV of the equatorial Pacific, which is an important element of the recharge–discharge paradigm of ENSO (e.g., Meinen and McPhaden 2000). According to observations, variations in the basinwide equatorial WWV lead SST variations in the eastern equatorial Pacific by roughly six months to one year. Figure 2b shows a nearly uniform deepening of the equatorial thermocline prior to an El Niño event consistent with these observations (in our idealized approach, the mean depth of the thermocline along the equator represents WWV). Here, we will investigate the phase difference between variations in the mean thermocline depth  $h_m$  and the temperature  $T_e$  of the eastern equatorial Pacific. We will also consider  $h_w$  and  $h_e$ , which correspond to WWV anomalies in the western and eastern Pacific.

The mean (zonally averaged) depth of the equatorial thermocline is defined as

$$h_m = \int_0^1 h(x) dx. \quad (8.1)$$

We have used the subscript  $m$  to distinguish averaging over the entire length of the basin from averaging applied over the eastern equatorial Pacific.

We can go back to the Fourier space (again, using the same notations for the corresponding variables) to obtain

$$h_m = \tau_o \left( r_m + q \sqrt{\frac{\varepsilon}{\varepsilon x_c + \alpha}} \right) T_e, \quad (8.2)$$

where

$$r_m = \int_0^1 R(x) dx. \quad (8.3)$$

Integrating Eq. (8.3) by parts and using Eqs. (4.3)–(4.4) give  $r_m = -q$ . Therefore, Eq. (8.2) can be rewritten as

$$T_e = (q\tau_o)^{-1} \left( \sqrt{\frac{\varepsilon}{\varepsilon x_c + \alpha}} - 1 \right)^{-1} h_m. \quad (8.4)$$

We now define

$$\begin{aligned} \phi = \phi(\omega) &= \arg \left( \sqrt{\frac{\varepsilon}{\varepsilon x_c + \alpha}} - 1 \right)^{-1} \\ &= -\arg \left( \sqrt{\frac{\varepsilon}{\varepsilon x_c + \alpha}} - 1 \right). \end{aligned} \quad (8.5)$$

Here,  $\phi$  is the phase difference between variations in  $h_m$  and  $T_e$ . Negative values of  $\phi$  would indicate that variations in  $h_m$  lead variations in  $T_e$  (i.e.,  $T_e$  is lagging  $h_m$ ).

We now set  $\varepsilon = \varepsilon_m + i\omega$  and assume that the oscillation is close to neutral stability, neglecting potential growth/decay rates (including the growth/decay rates would be equivalent to modifying  $\varepsilon_m$ ), so that

$$\phi = -\arg \left[ \sqrt{\frac{\varepsilon_m + i\omega}{(\varepsilon_m + i\omega)x_c + \alpha}} - 1 \right]. \quad (8.6)$$

Even though this expression was derived within the shallow-water equations, it has a universal character since it depends only on the oscillation frequency, oceanic damping, and the structure of wind stress anomalies (i.e., their meridional extent and the location of wind maximum). To the leading order, this expression neither depends on the zonal extent of the wind anomalies nor on their amplitude, and is more general than the results of the simple model in Fig. 5.

Figure 7 shows the dependence of the phase lag  $\phi$  on the oscillation period  $T = 2\pi/\omega$  for various values of the wind stress curl parameter  $\alpha$ . For realistic combinations of  $\alpha$  and  $\varepsilon_m$  and for the range of periods relevant to ENSO, the phase difference increases with the oscillation period but typically remains smaller than  $90^\circ$ . For example, for  $T = 4$  yr and our standard combination of  $\alpha$  and  $\varepsilon_m$ , the model gives  $|\phi| \approx 60^\circ$  or approximately eight months. Decreasing  $\alpha$  and hence reducing the meridional Sverdrup flow or increasing oceanic damping rates reduces the lag (Fig. 8).

Many coupled GCMs produce wind stress anomalies confined too close to the equator (Capotondi et al. 2006; Deser et al. 2006), which corresponds to too-large values

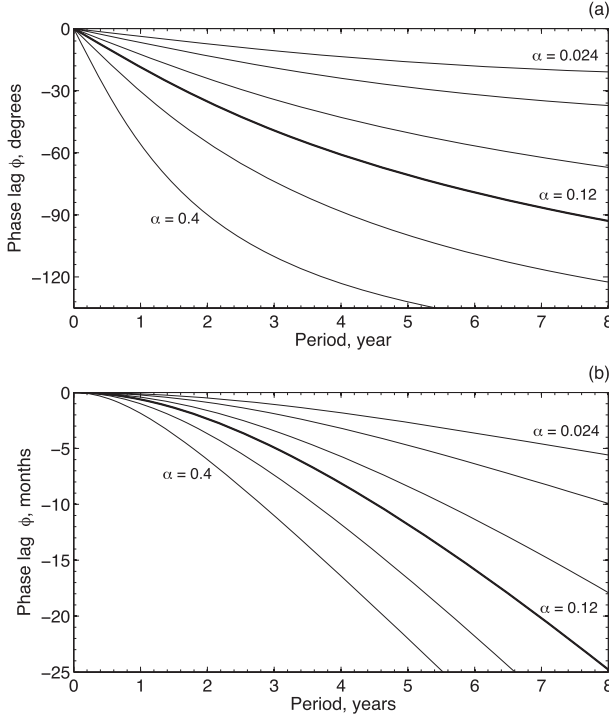


FIG. 7. The phase lag  $\phi$  between variations in the temperature of the eastern equatorial Pacific  $T_e$  and the mean thermocline depth  $h_m$ , as measured in (a) degrees and (b) months. Negative values indicate that  $T_e$  lags  $h_m$ . Different lines correspond to different values of the meridional extent of wind stress anomalies (i.e., different values of  $\alpha$ ). From the bottom line to the top: the wind stress meridional decay scales are  $5^\circ$ ,  $7^\circ$ ,  $9^\circ$ ,  $11^\circ$ ,  $15^\circ$ , and  $20^\circ$  of latitude ( $\alpha = 0.4, 0.2, 0.12, 0.08, 0.043, 0.024$ ). The thick line corresponds to the standard case with  $\alpha = 0.12$ . For  $\varepsilon_m = 0.1$  and  $x_c = 0.4$ .

of  $\alpha$ . Figures 7 and 8 suggest that the phase lag between the WWV and the temperature in the Niño-3 region for these models can become too large, even greater than  $90^\circ$ , unless the effect of  $\alpha$  on the phase lag is counteracted by strong oceanic damping rates or a too-short period of the simulated oscillation.

Next, to take into account the entire range of available frequencies, we apply the inverse Fourier transform to Eq. (8.2) and arrive at a full expression for the mean thermocline depth  $h_m$  in terms of an integral operator applied to  $T_e$ . Similar expressions are obtained for  $h_e$  and  $h_w$  (thermocline depths in the eastern and western equatorial Pacific, respectively):

$$h_m = \tau_o q \left[ \left( \frac{1}{\sqrt{x_c}} - 1 \right) T_e + \frac{1}{\pi \sqrt{x_c}} \int_0^\infty e^{-\varepsilon_m t'} I(\hat{\alpha}, t') T_e(t - t') dt' \right], \quad (8.7)$$

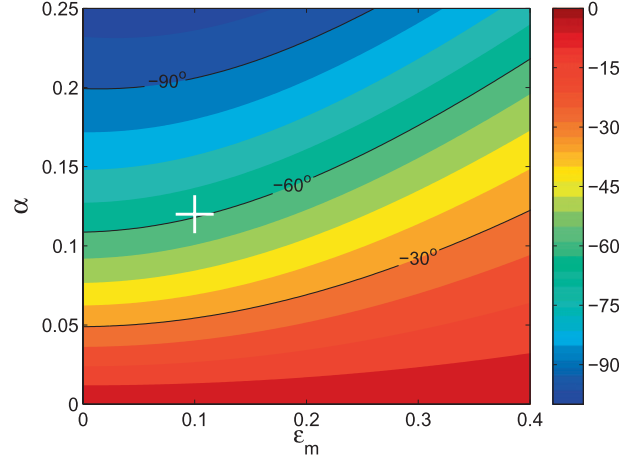


FIG. 8. The phase lag  $\phi$  ( $^\circ$ ) between variations in the temperature of the eastern equatorial Pacific  $T_e$  and  $h_m$  as a function of  $\varepsilon_m$  and  $\alpha$ , for the period of the oscillation  $T = 4$  yr. Negative values of  $\phi$  mean that  $T_e$  lags  $h_m$ . The three contour lines correspond to the lag  $\phi = -90^\circ$ ,  $-60^\circ$ ,  $-30^\circ$ . The white cross indicates standard tropical conditions with  $\varepsilon_m = 0.1$  and  $\alpha = 0.12$ . For  $x_c = 0.4$ .

$$h_e = \tau_o q \left[ \left( \frac{r}{q} + \frac{1}{\sqrt{x_c}} \right) T_e + \frac{1}{\pi \sqrt{x_c}} \int_0^\infty e^{-\varepsilon_m t'} I(\hat{\alpha}, t') T_e(t - t') dt' \right], \quad \text{and} \quad (8.8)$$

$$h_w = \tau_o q \left[ \left( -2 - \frac{r}{q} + \frac{1}{\sqrt{x_c}} \right) T_e + \frac{1}{\pi \sqrt{x_c}} \int_0^\infty e^{-\varepsilon_m t'} I(\hat{\alpha}, t') T_e(t - t') dt' \right]. \quad (8.9)$$

These expressions allow us to calculate changes in  $h_m$ ,  $h_e$ , and  $h_w$  for a given structure of wind stress anomalies and fixed oceanic damping rates if temperature variations in the eastern equatorial Pacific are known. Note that Eq. (8.8) was already derived in section 4. Averaging in Eq. (8.9) is done over the western half of the Pacific basin. For a realistic combination of parameters, the largest contribution to  $h_e$  comes from the term proportional to  $T_e$ , whereas the expression for  $h_w$  is dominated by the second term.

The results of calculations are shown in Fig. 9, for which the thermocline depths were calculated using the observed Niño-3 SST in place of  $T_e$  (Fig. 9a). Comparison between computed  $h_m$ ,  $h_e$ , and  $h_w$  and observed WWV variations demonstrates a very good agreement, especially for such an idealized linear model based on several approximations with the low-frequency limit being

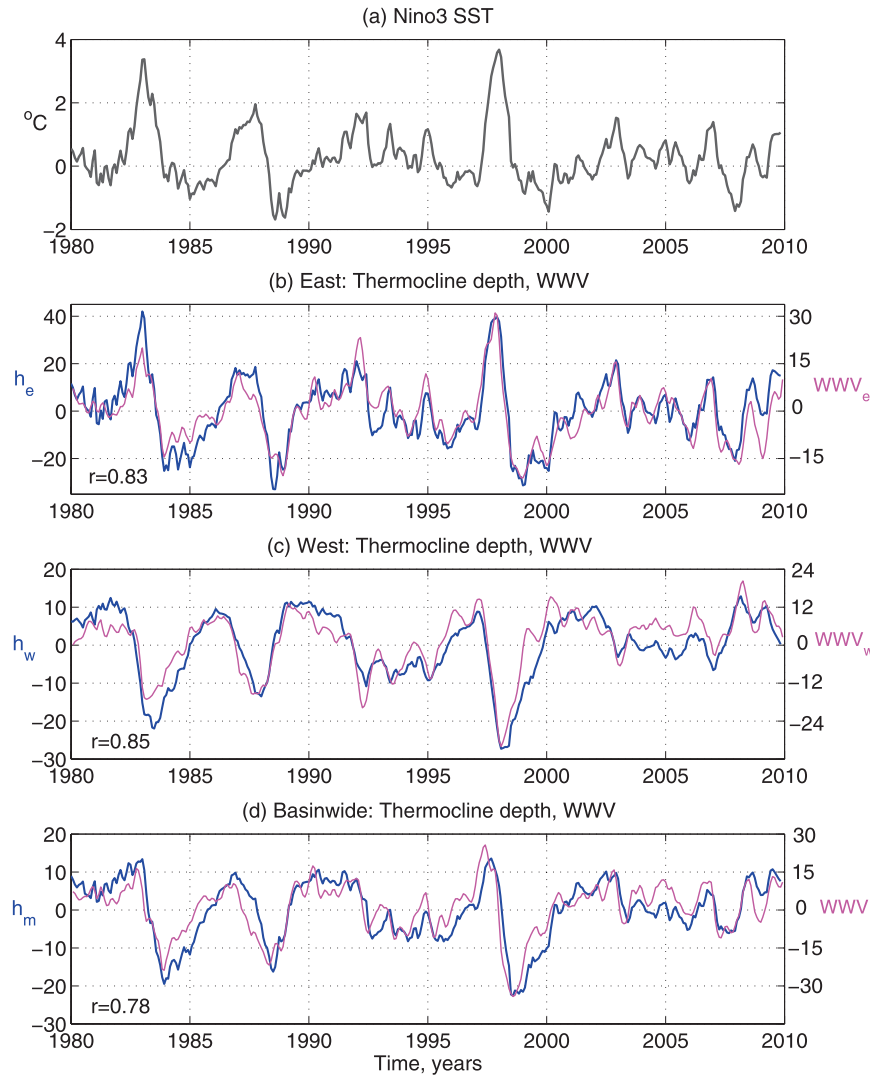


FIG. 9. (a) Variations in the Niño-3 SST from the extended dataset of Kaplan et al. 1998. (b)–(d) Variations in the thermocline depth (blue, m) and the WWV (magenta,  $m^3 \times 10^{13}$ ) in the eastern, western, and the basinwide equatorial Pacific, respectively. Thermocline depths are calculated using the low-frequency approximation, Eqs. (8.7)–(8.9), and the observed Niño-3 SST in place of  $T_e$ . Correlation coefficients between thermocline depth variations and WWV are shown in the bottom-left corner of each panel. Note that the scaling of WWV variations is different for each case. The WWV data (integrated between  $5^\circ\text{S}$  and  $5^\circ\text{N}$ ) are from the Tropical Atmosphere Ocean Project (TAO, see <http://www.pmel.noaa.gov/tao/elni/o/wwv>). The non-dimensional parameters are  $\epsilon_m = 0.1$ ,  $\alpha = 0.12$ , and  $x_c = 0.4$ .

one of them. The correlation between the observed  $h_w$  and calculated WWV in the west reaches 0.85, indicating that our approximation captures ocean heat recharge in the western tropical Pacific quite nicely.

## 9. Discussion and conclusions

In this study we have proposed the low-frequency limit as a useful approximation to describe the ocean response to slow wind variations and ENSO dynamics

in general. Using this limit, we have formally derived a model of ENSO based on a simple integro-differential equation that uses an integral operator to compute the ocean adjustment. The derivation is based on expanding the shallow-water equations into the powers of a small parameter  $\epsilon$ , which is related to the ratio  $T_k/T$  and the oceanic damping rate  $\epsilon_m$  ( $T_k$  is the time needed for a Kelvin wave to cross the Pacific).

The proposed approach efficiently integrates the effects of equatorial Kelvin and Rossby waves of different

modes, thus eliminating the necessity to treat these waves explicitly and providing an analytical expression for spatial and temporal changes in the thermocline depth. When averaged over the eastern equatorial Pacific, this expression reduces to a formula for the thermocline anomaly  $h_e$  as a function of SST variations in the eastern Pacific. Used together with an approximate SST equation along the equator, this description of thermocline depth anomalies leads to our model of ENSO in the low-frequency limit.

The method has some parallels with the fast-wave limit of ENSO (Neelin 1991; Hao et al. 1993; Cane 1992). However, the original fast-wave limit treats ocean waves as instantaneous and hence does not take into account the time necessary for the ocean thermocline to adjust (thus neglecting ocean memory). As a result, that limit produces unrealistic oscillations (Galanti and Tziperman 2000). In contrast, our approach, while also assuming that the ENSO period is much longer than wave time scales, does allow for the slow ocean adjustment, thereby incorporating the essential physics of ENSO related to the delayed or recharge/discharge dynamics.

How accurate is the low-frequency approximation? The commonly accepted range of the ENSO-like climate variability is 2–7 yr. For oceanic damping time scale of approximately two years, this gives the range of the expansion parameter  $|\varepsilon|$  from approximately 0.2 to 0.6. The longer the period, the smaller this parameter is. Since the late 1970s (e.g., Fedorov and Philander 2000, 2001), the dominant ENSO period has been 5 yr ( $|\varepsilon| \approx 0.25$ ), which is reasonably small for applying the low-frequency approximation. For decadal climate variations and ocean response to steady wind forcing,  $\varepsilon$  is  $O(0.1)$ , which makes the method even more accurate.

Moreover, the leading-order expansion term for thermocline anomalies is even more accurate than one might think just estimating the magnitude of  $|\varepsilon|$ . The reason is twofold: first, the first term of the expansion is  $O(1)$ , whereas the next-order term is already proportional to  $\varepsilon^2$ ; and second, higher-order corrections to the thermocline depth (appendix A) affect the thermocline only at some distance away from the equator (several Rossby radii) and thus do not modify the dominant, large-scale pattern of the ocean response to wind stress. A comparison of our leading-order expression with the full solution of the shallow-water equations indicates that the low-frequency limit may work well even for periods of the forcing close to one year.

Whereas the present paper considers only wind perturbations that are zonal and centered along the equator, a complimentary study (M. Parker and A. V. Fedorov 2010, unpublished manuscript) extends the

low-frequency limit onto arbitrary wind forcing with both zonal and meridional components. Our model of ENSO in the low-frequency limit yields simple algebraic constraints on the frequency and growth or decay rate of ENSO-like oscillations. In particular, the results clearly show that how the interplay between the curl of wind stress anomalies and oceanic damping rates affect both the periodicity and the growth (or decay) of the ENSO mode. The importance of the meridional wind structure, and hence the wind stress curl, and oceanic damping rates for ENSO dynamics has been emphasized recently by other authors as well (Capotondi et al. 2006; Clarke et al. 2007; Brown and Fedorov 2010b).

With further simplifications, our model can be reduced to either a delayed or recharge oscillator. In the latter case the recharge oscillator would explicitly include the effect of the wind stress curl. These new derivations are more accurate mathematically than the original derivations; they also highlight the limitations of the traditional ENSO paradigms and explain why those paradigms, while very useful conceptually, do not necessarily produce sufficient quantitative agreement when compared to comprehensive coupled models or observations (Mechoso et al. 2003). Thus, the proposed simple model of ENSO in the low-frequency limit gives a quantitatively more rigorous alternative to the traditional models of ENSO.

As part of calculations, we have derived a simple analytical expression for the phase lag between SST variations in the eastern equatorial Pacific and variations in the mean thermocline depth along the equator (the equatorial warm water volume and ocean heat content are useful proxies for this depth). This phase lag is an essential element of the ocean recharge–discharge physics during the ENSO cycle. We show that the lag critically depends on the frequency of the oscillation, the wind stress curl and oceanic damping rates, and is not necessarily equal to  $90^\circ$  as sometimes assumed. In fact, for an oscillation with a 4-yr period and close to neutral stability, the model predicts a phase difference of roughly  $60^\circ$  for typical oceanic conditions.

Our results demonstrate that the low-frequency limit is a useful approximation that can be applied in a broad range of frequencies of the wind stress forcing—from nearly annual to decadal (and for considering ocean response to steady winds). The method also provides explicit expressions for estimating interannual changes in the mean depth of the equatorial thermocline (and hence the equatorial warm water volume) and thermocline depth variations in the eastern and western equatorial Pacific. A good agreement between the observed variations in WWV and those hindcast by our method gives another justification for the low-frequency approximation.

**Acknowledgments.** This research was supported by NSF (Grants OCE-0550439 and OCE-0901921), the DOE Office of Science (Grant DE-FG02-08ER64590), and the Packard Foundation. This work began at Princeton University, continued at Yale, and was first presented at the summer GFD School at WHOI in 2005.

## APPENDIX A

### Higher-Order Corrections for $h$

We start from the two equations derived in the main body of the paper for  $h$  and  $u$ :

$$h_x - \varepsilon y^2 h = (1 - y\partial_y) \tau - \varepsilon(1 - y\partial_y) u \quad \text{and} \quad (\text{A.1})$$

$$u = -h_y/y. \quad (\text{A.2})$$

Assuming that  $|\varepsilon|$  is a small parameter, we expand  $h$  and  $u$  in powers of  $\varepsilon$ :

$$h = h^{(0)} + h^{(2)} + \dots \quad \text{and} \quad (\text{A.3})$$

$$u = u^{(1)} + u^{(3)} + \dots, \quad (\text{A.4})$$

where the terms in Eqs. (A.3) and (A.4) are proportional to powers of  $\varepsilon$  as indicated by the superscripts. The terms proportional to odd and even powers of  $\varepsilon$  fall out from the series for  $h$  and  $u$ , respectively, as long as the solutions are symmetrical with respect to the equator.

Formally, as discussed in section 3, a constraint on the basin size could be imposed such that  $|y| < Y$ , where  $Y \sim \varepsilon^{-1/2}$ , to keep the second term on the left-hand-side of Eq. (A.1) not larger than  $O(1)$ . However, as we will show next, the solutions for  $h$  decay exponentially for large  $|y|$  as long as  $x \neq 0$ , so that this constraint can be relaxed.

Using Eqs. (A.3) and (A.4) in Eqs. (A.1) and (A.2) yields a set of recurrent equations for different terms of the expansion as

$$h_x^{(2n)} - \varepsilon y^2 h^{(2n)} = (1 - y\partial_y) \tau^{(2n)} \quad \text{and} \quad (\text{A.5})$$

$$u^{(2n+1)} = -h_y^{(2n)}/y, \quad \text{with} \quad (\text{A.6})$$

$$\tau^{(n)} = \begin{cases} \tau & \text{for } n = 0 \\ -\varepsilon u^{(2n-1)} & \text{for } n = 1, 2, 3 \dots \end{cases} \quad (\text{A.7})$$

Similar to the expressions in the main body of the text, their solutions are

$$h^{(2n)} = e^{\varepsilon y^2(x-1)} h_{2n} - \int_x^1 e^{\varepsilon y^2(x-s)} (1 - y\partial_y) \tau^{(2n)} ds \quad \text{and} \quad (\text{A.8})$$

$$u^{(2n+1)} = 2\varepsilon(1-x)e^{\varepsilon y^2(x-1)} h_{2n} - \int_x^1 e^{\varepsilon y^2(x-s)} [\partial_{yy} + 2\varepsilon(s-x)(1-y\partial_y)] \tau^{(2n)} ds \quad \text{with} \quad (\text{A.9})$$

$$h_{2n} = \pi^{-1/2} \varepsilon^{1/2} \int_0^1 \int_{-\infty}^{\infty} \tau^{(2n)} e^{-\varepsilon y^2 s} s ds dy. \quad (\text{A.10})$$

When calculating these integrals, in the terms  $\tau^{(2n)}(x, y)$ , variable  $x$  should be replaced with  $s$ . We have assumed that  $\tau_{yy}^{(2n)} \leq O(\varepsilon)$ . Note that both  $h$  and  $u$  decay exponentially for large  $|y|$ , as long as  $x \neq 1$ , while  $u$  is identically zero for  $x = 1$  (i.e., at the eastern boundary). In principle, Eqs. (A.7)–(A.10) solve the problem completely.

Calculating the first few terms in the expansion gives

$$h^{(0)} = e^{\varepsilon y^2(x-1)} h_o - \int_x^1 e^{\varepsilon y^2(x-s)} (1 - y\partial_y) \tau ds \quad \text{and} \quad (\text{A.11})$$

$$u^{(1)} = 2\varepsilon(1-x)e^{\varepsilon y^2(x-1)} h_o - \int_x^1 e^{\varepsilon y^2(x-s)} [\partial_{yy} + 2\varepsilon(s-x)(1-y\partial_y)] \tau ds \quad \text{with} \quad (\text{A.12})$$

$$h_o = \pi^{-1/2} \varepsilon^{1/2} \int_0^1 \int_{-\infty}^{\infty} \tau e^{-\varepsilon y^2 s} s ds dy. \quad (\text{A.13})$$

The next order terms are

$$h^{(2)} = e^{\varepsilon y^2(x-1)} h_2 + \varepsilon \int_x^1 e^{\varepsilon y^2(x-s)} (1 - y\partial_y) u^{(1)} ds \quad \text{and} \quad (\text{A.14})$$

$$u^{(3)} = 2\varepsilon(1-x)e^{\varepsilon y^2(x-1)} h_2 + \varepsilon \int_x^1 e^{\varepsilon y^2(x-s)} [\partial_{yy} + 2\varepsilon(s-x)(1-y\partial_y)] u^{(1)} ds \quad \text{with} \quad (\text{A.15})$$

$$h_2 = \pi^{-1/2} \varepsilon^{3/2} \int_0^1 \int_{-\infty}^{\infty} u^{(1)} e^{-\varepsilon y^2 s} s ds dy. \quad (\text{A.16})$$

Assuming that

$$\tau = \tau(s) e^{-\alpha y^2}, \quad (\text{A.17})$$

we obtain

$$h_o = \int_0^1 \frac{s}{(s + \alpha/\varepsilon)^{1/2}} \tau(s) ds, \quad (\text{A.18})$$

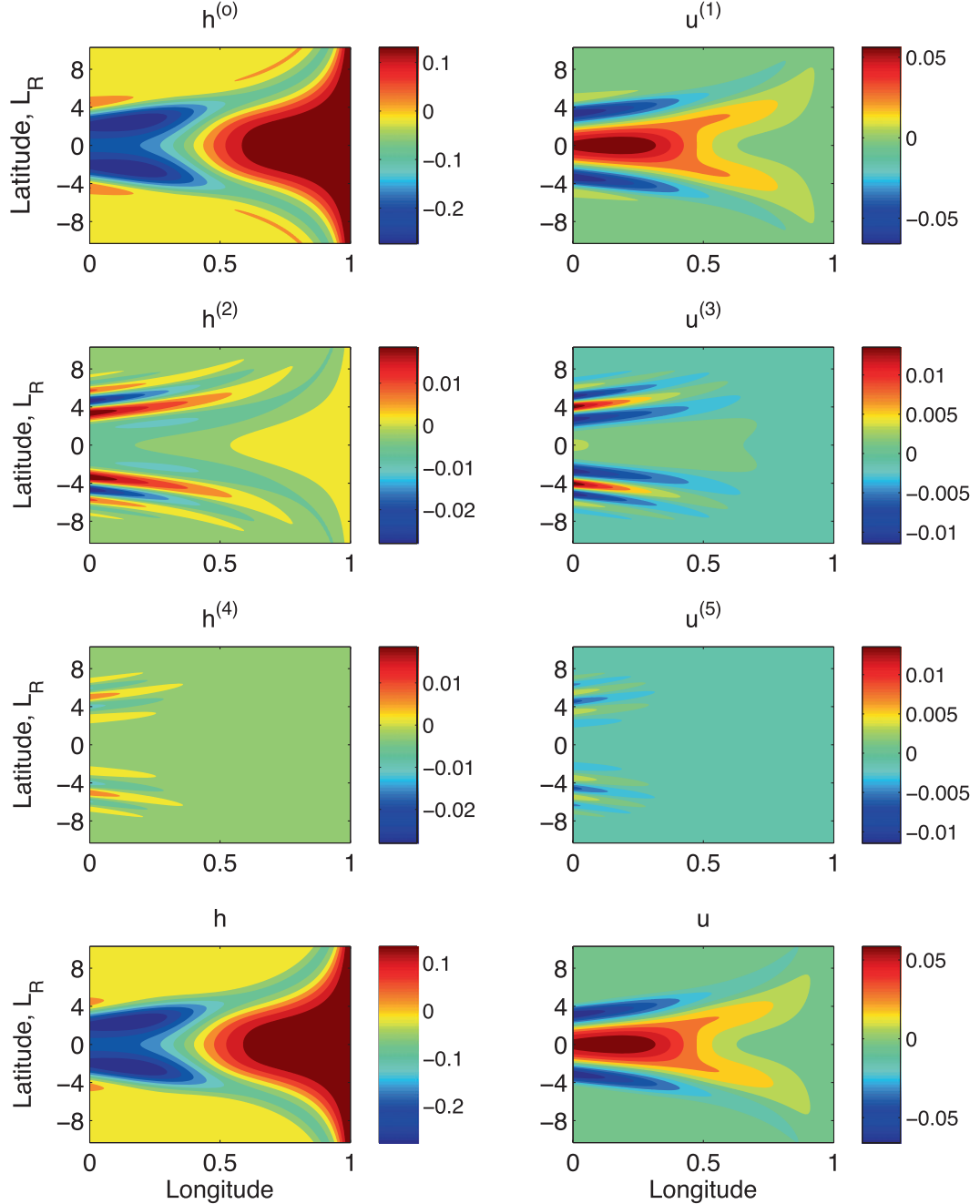


FIG. A1. The first three terms of the low-frequency expansion for (left) thermocline and (right) zonal velocity anomalies and the resultant  $h$  and  $u$  for the oscillation period  $T = 4$  yr. Only the real parts of  $h$  and  $u$  are shown (both variables, longitude and latitude are nondimensionalized). The spatial structure of the imposed wind stress as in Fig. 2c. The nondimensional parameters are  $\varepsilon_m = 0.1$ ,  $\tau_o = 1$ ,  $\alpha = 0.12$ ,  $x_c = 0.4$ , and  $\nu = 25$ .

$$\begin{aligned} h_2 = & -\frac{1}{3}\varepsilon^2 h_o + 2\varepsilon^2 \int_0^1 \int_s^1 \frac{(p-s)s}{(p+\alpha/\varepsilon)^{1/2}} \tau(p) dp ds \\ & + 2\varepsilon^2 \int_0^1 \int_s^1 \frac{ps^2}{(p+\alpha/\varepsilon)^{3/2}} \tau(p) dp ds, \end{aligned} \quad (\text{A.19})$$

and so on.

Figure A1 shows the first three terms in the expansion Eqs. (A.3) and (A.4) and the resultant  $h$  and  $u$  obtained by adding these terms together. The higher-order corrections are rather small, and for practical purposes just one or two first terms of the expansion are sufficient.

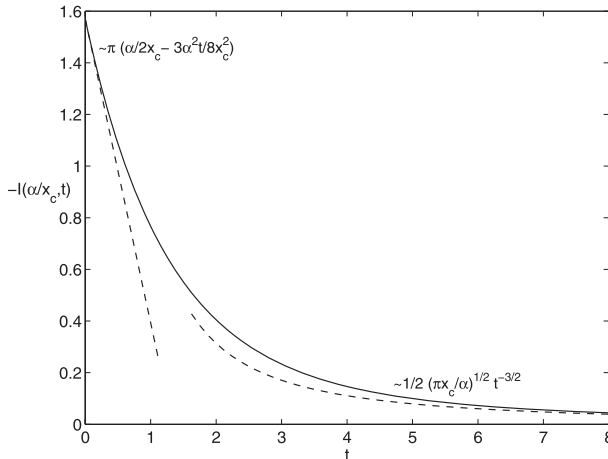


FIG. B1. The plot of the function  $-I(\hat{\alpha}/x_c, t)$  calculated from Eq. (B.1) and its asymptotes for small and large  $t$ . Here, this function is plotted for  $\alpha = 1$ .

## APPENDIX B

### Estimating the Integral $I(\hat{\alpha}, t)$

Here, we consider the properties and the asymptotes of the integral  $I(\hat{\alpha}, t)$  used in the kernel of the integro-differential operator in Eq. (4.12):

$$I(\hat{\alpha}, t) = \frac{d}{dt} I_1(\hat{\alpha}t) = \frac{d}{dt} \int_0^1 \frac{e^{-\hat{\alpha}ts}}{\sqrt{s(1-s)}} ds. \quad (\text{B.1})$$

For large  $t$

$$\begin{aligned} I(\hat{\alpha}, t) &\sim \frac{d}{dt} \int_0^1 \frac{e^{-\hat{\alpha}ts}}{\sqrt{s}} ds \sim \frac{d}{dt} \int_0^\infty \frac{e^{-\hat{\alpha}ts}}{\sqrt{s}} ds \\ &= 2 \frac{d}{dt} \int_0^\infty e^{-\hat{\alpha}ts^2} ds = \frac{d}{dt} \sqrt{\frac{\pi}{t\hat{\alpha}}} = -\frac{1}{2} \left(\frac{\pi}{\hat{\alpha}}\right)^{1/2} t^{-3/2}. \end{aligned} \quad (\text{B.2})$$

For small  $t$

$$\begin{aligned} I(\hat{\alpha}, t) &= \frac{d}{dt} \int_0^1 \frac{1 - \hat{\alpha}ts + 1/2(\hat{\alpha}ts)^2 - \dots}{\sqrt{s(1-s)}} ds \\ &= \frac{d}{dt} \pi \left(1 - \frac{\hat{\alpha}t}{2} + \frac{3\hat{\alpha}^2t^2}{16} - \dots\right) \approx -\pi \left(\frac{\hat{\alpha}}{2} - \frac{3\hat{\alpha}^2t}{8}\right), \end{aligned} \quad (\text{B.3})$$

where

$$\hat{\alpha} = \alpha/x_c. \quad (\text{B.4})$$

Figure B1 shows the behavior of  $I(\hat{\alpha}, t)$  evaluated numerically.

## REFERENCES

- Battisti, D. S., 1988: Dynamics and thermodynamics of a warming event in a coupled tropical atmosphere–ocean model. *J. Atmos. Sci.*, **45**, 2889–2919.
- , and A. C. Hirst, 1989: Interannual variability in a tropical atmosphere–ocean model: Influence of the basic state, ocean geometry and nonlinearity. *J. Atmos. Sci.*, **46**, 1687–1712.
- Behringer, D. W., M. Ji, and A. Leetmaa, 1998: An improved coupled model for ENSO prediction and implications for ocean initialization. Part I: The ocean data assimilation system. *Mon. Wea. Rev.*, **126**, 1013–1021.
- Brown, J. N., and A. V. Fedorov, 2008: The mean energy balance in the tropical ocean. *J. Mar. Res.*, **66**, 1–23.
- , and —, 2010a: Estimating the diapycnal transport contribution to warm water volume variations in the tropical Pacific Ocean. *J. Climate*, **23**, 221–237.
- , and —, 2010b: How much energy is transferred from the winds to the thermocline on ENSO time scales? *J. Climate*, **23**, 1563–1580.
- Cane, M. A., 1992: Comments on “The fast-wave limit and interannual oscillations.” *J. Atmos. Sci.*, **49**, 1947–1949.
- , and E. S. Sarachik, 1977: Forced baroclinic ocean motions: II. The linear equatorial bounded case. *J. Mar. Res.*, **35**, 395–432.
- , and D. W. Moore, 1981: A note on low-frequency equatorial basin modes. *J. Phys. Oceanogr.*, **11**, 1578–1584.
- , and E. S. Sarachik, 1981: The response of a linear baroclinic equatorial ocean to periodic forcing. *J. Mar. Res.*, **39**, 651–693.
- , M. Münnich, and S. E. Zebiak, 1990: A study of self-excited oscillations of the tropical ocean–atmosphere system. Part I: Linear analysis. *J. Atmos. Sci.*, **47**, 1562–1577.
- Capotondi, A., A. Wittberg, and S. Masina, 2006: Spatial and temporal structure of Tropical Pacific interannual variability in 20th century coupled simulations. *Ocean Model.*, **15**, 274–298.
- Clarke, A. J., 1992: Low-frequency reflection from a nonmeridional eastern ocean boundary and the use of coastal sea level to monitor eastern Pacific equatorial Kelvin waves. *J. Phys. Oceanogr.*, **22**, 163–183.
- , 2008: *An Introduction to the Dynamics of El Niño & the Southern Oscillation*. Elsevier, 324 pp.
- , 2010: Analytical theory for the quasi-steady and low-frequency equatorial ocean response to wind forcing: The tilt and warm water volume modes. *J. Phys. Oceanogr.*, **40**, 121–137.
- , S. Van Gorder, and G. Colantuono, 2007: Wind stress curl and ENSO discharge/recharge in the equatorial Pacific. *J. Phys. Oceanogr.*, **37**, 1077–1091.
- Deser, C., A. Capotondi, R. Saravanan, and A. S. Phillips, 2006: Tropical Pacific and Atlantic climate variability in CCSM3. *J. Climate*, **19**, 2451–2481.
- Fedorov, A. V., 2002: The response of the coupled tropical ocean–atmosphere to westerly wind bursts. *Quart. J. Roy. Meteor. Soc.*, **128**, 1–23.
- , 2007: Net energy dissipation rates in the tropical ocean and ENSO dynamics. *J. Climate*, **20**, 1099–1108.
- , and S. G. Philander, 2000: Is El Niño changing? *Science*, **288**, 1997–2002.
- , and S. G. H. Philander, 2001: A stability analysis of the tropical ocean–atmosphere interactions: Bridging measurements and theory for El Niño. *J. Climate*, **14**, 3086–3101.

- , and J. Brown, 2009: Equatorial waves. *Encyclopedia of Ocean Sciences*, J. Steele, Ed., Academic Press, 3679–3695.
- , S. L. Harper, S. G. H. Philander, B. Winter, and A. Wittenberg, 2003: How predictable is El Niño? *Bull. Amer. Meteor. Soc.*, **84**, 911–919.
- Galanti, E., and E. Tziperman, 2000: ENSO's phase locking to the seasonal cycle in the fast-SST, fast-wave, and mixed-mode regimes. *J. Atmos. Sci.*, **57**, 2936–2950.
- Guilyardi, E., A. Wittenberg, A. Fedorov, M. Collins, C. Wang, A. Capotondi, G. J. van Oldenborgh, and T. Stockdale, 2009: Understanding El Niño in ocean–atmosphere general circulation models: Progress and challenges. *Bull. Amer. Meteor. Soc.*, **90**, 325–340.
- Hao, Z., J. D. Neelin, and F.-F. Jin, 1993: Nonlinear tropical air–sea interaction in the fast-wave limit. *J. Climate*, **6**, 1523–1544.
- Jin, F.-F., 1997a: An equatorial ocean recharge paradigm for ENSO. Part I: Conceptual model. *J. Atmos. Sci.*, **54**, 811–829.
- , 1997b: An equatorial ocean recharge paradigm for ENSO. Part II: A stripped-down coupled model. *J. Atmos. Sci.*, **54**, 830–847.
- , 2001: Low-frequency modes of tropical ocean dynamics. *J. Climate*, **14**, 3874–3881.
- , and J. D. Neelin, 1993: Modes of interannual tropical ocean–atmosphere interaction—A unified view. Part I: Numerical results. *J. Atmos. Sci.*, **50**, 3477–3503.
- , and S.-I. An, 1999: Thermocline and zonal advective feedbacks within the equatorial ocean recharge oscillator model for ENSO. *Geophys. Res. Lett.*, **26**, 2989–2992.
- Johnson, G. C., M. J. McPhaden, and E. Firing, 2001: Equatorial Pacific ocean horizontal velocity, divergence, and upwelling. *J. Phys. Oceanogr.*, **31**, 839–849.
- Kaplan, A., M. Cane, Y. Kushnir, A. Clement, M. Blumenthal, and B. Rajagopalan, 1998: Analyses of global sea surface temperature 1856–1991. *J. Geophys. Res.*, **103**, 18 567–18 589.
- Kessler, W. S., 2003: Is ENSO a cycle or a series of events? *Geophys. Res. Lett.*, **29**, 2125, doi:10.1029/2002GL015924.
- McCreary, J. P., 1985: Modeling equatorial ocean circulation. *Annu. Rev. Fluid Mech.*, **17**, 359–409.
- Mechoso, C., J. D. Neelin, and J.-Y. Yu, 2003: Testing simple models of ENSO. *J. Atmos. Sci.*, **60**, 305–318.
- Meinen, C. S., and M. J. McPhaden, 2000: Observations of warm water volume changes in the equatorial Pacific and their relationship to El Niño and La Niña. *J. Climate*, **13**, 3551–3559.
- , —, and G. C. Johnson, 2001: Vertical velocities and transports in the equatorial Pacific during 1993–99. *J. Phys. Oceanogr.*, **31**, 3230–3248.
- Münnich, M., M. A. Cane, and S. E. Zebiak, 1991: A study of self-excited oscillations of the tropical ocean–atmosphere system. Part II: Nonlinear cases. *J. Atmos. Sci.*, **48**, 1238–1248.
- Neelin, J. D., 1991: The slow sea surface temperature mode and the fast-wave limit: Analytic theory for tropical interannual oscillations and experiments in a hybrid coupled model. *J. Atmos. Sci.*, **48**, 584–606.
- , D. S. Battisti, A. C. Hirst, F.-F. Jin, Y. Wakata, T. Yamagata, and S. E. Zebiak, 1998: ENSO theory. *J. Geophys. Res.*, **103**, 14 261–14 290.
- Philander, S. G. H., and A. V. Fedorov, 2003: Is El Niño sporadic or cyclic? *Annu. Rev. Earth Planet. Sci.*, **31**, 579–594.
- Schopf, P. S., and M. J. Suarez, 1988: Vacillations in a coupled ocean–atmosphere model. *J. Atmos. Sci.*, **45**, 549–566.
- Stricherz, J. N., D. M. Legler, and J. J. O'Brien, 1997: Tropical Pacific Ocean. Vol. 2, TOGA Pseudo-Stress Atlas 1985–1994, COAPS Tech. Rep. 97-2, 177 pp. [Available from COAPS, The Florida State University, Tallahassee, FL 32306.]
- Suarez, M. J., and P. S. Schopf, 1988: A delayed action oscillator for ENSO. *J. Atmos. Sci.*, **45**, 3283–3287.
- Wang, C., 2001: A unified oscillator model for the El Niño–Southern Oscillation. *J. Climate*, **14**, 98–115.
- , S.-P. Xie, and J. A. Carton, Eds., 2004: *Earth's Climate: The Ocean–Atmosphere Interaction*. Geophys. Monogr., Vol. 147, Amer. Geophys. Union, 405 pp.
- Wittenberg, A. T., 2004: Extended wind stress analyses for ENSO. *J. Climate*, **17**, 2526–2540.
- Zakharov, V. E., 1968: Stability of periodic waves of finite amplitude on the surface of a deep fluid. *J. Appl. Mech. Tech. Phys.*, **9**, 190–194, doi:10.1007/BF00913182.
- Zebiak, S. E., and M. A. Cane, 1987: A model El Niño–Southern Oscillation. *Mon. Wea. Rev.*, **115**, 2262–2278.